

RESEARCH

Open Access



Early tau detection in flortaucipir images: validation in autopsy-confirmed data and implications for disease progression

Vikas Kotari*, Sudeepti Southeikal, Michael Navitsky, Ian A. Kennedy, Ming Lu, Amanda Morris, Jennifer Ann Zimmer, Adam S. Fleisher, Mark A. Mintun, Michael D. Devous Sr and Michael J. Pontecorvo

Abstract

Background There is an increasing interest in utilizing tau PET to identify patients early in Alzheimer's disease (AD). In this work, a temporal lobe composite (Et) volume of interest (VOI) was evaluated in a longitudinal flortaucipir cohort and compared to a previously described global neocortical VOI. In a separate autopsy-confirmed study, the sensitivity of the Et VOI for identifying intermediate (B2) neurofibrillary tangle (NFT) pathology was evaluated.

Methods A total of 427 subjects received flortaucipir, florbetapir, MRI, and cognitive evaluation at baseline and 18 months. In a separate autopsy study, 67 subjects received ante-mortem flortaucipir scans, and neuropathological findings were recorded according to NIA-AA recommendations by two experts. Two VOIs: Et comprising FreeSurfer volumes (bilateral entorhinal cortex, fusiform, parahippocampal, and inferior temporal gyri) transformed to MNI space and a previously published global AD signature-weighted neocortical VOI ($AD_{signature}$) (Devous et al., *J Nucl Med* 59:937–43, 2018), were used to calculate SUVr relative to a white matter reference region (PERSI) (Southeikal et al., *J Nucl Med Off Publ Soc Nucl Med* 59:944–51, 2018). SUVr cutoffs for positivity were determined based on a cohort of young, cognitively normal subjects. Subjects were grouped based on positivity on both VOIs ($Et+/AD_{signature}+$; $Et+/AD_{signature}-$; $Et-/AD_{signature}-$). Groupwise comparisons were performed for baseline SUVr, 18-month changes in SUVr, neurodegeneration, and cognition. For the autopsy study, the sensitivity of Et in identifying intermediate Braak pathology (B2) subjects was compared to that of AD signature-weighted neocortical VOI. The average surface maps of subjects in the $Et+/AD_{signature}-$ group and B2 NFT scores were created for visual evaluation of uptake.

Results Sixty-four out of 390 analyzable subjects were identified as $Et+/AD_{signature}-$: 84% were $A\beta+$, 100% were diagnosed as MCI or AD, and 59% were $APOE \epsilon 4$ carriers. Consistent with the hypothesis that $Et+/AD_{signature}-$ status reflects an early stage of AD, $Et+/AD_{signature}-$ subjects deteriorated significantly faster than $Et-/AD_{signature}-$ subjects, but significantly slower than $Et+/AD_{signature}+$ subjects, on most measures (i.e., change in $AD_{signature}$ SUVr, Et ROI cortical thickness, and MMSE). The $AD_{signature}$ VOI was selective for subjects who came to autopsy with a B3 NFT score. In the autopsy study, 12/15 B2 subjects (including 10/11 Braak IV) were $Et+/AD_{signature}-$. Surface maps showed that flortaucipir uptake was largely captured by the Et VOI regions in B2 subjects.

Conclusion The Et VOI identified subjects with elevated temporal but not global tau ($Et+/AD_{signature}-$) that were primarily $A\beta+$, $APOE \epsilon 4$ carriers, and diagnosed as MCI or AD. $Et+/AD_{signature}-$ subjects had greater accumulation of tau, greater atrophy, and higher decline on MMSE in 18 months compared to $Et-/AD_{signature}-$ subjects. Finally, the Et VOI

*Correspondence:

Vikas Kotari

kotari@lilly.com

Full list of author information is available at the end of the article



© The Author(s) 2023. **Open Access** This article is licensed under a Creative Commons Attribution 4.0 International License, which permits use, sharing, adaptation, distribution and reproduction in any medium or format, as long as you give appropriate credit to the original author(s) and the source, provide a link to the Creative Commons licence, and indicate if changes were made. The images or other third party material in this article are included in the article's Creative Commons licence, unless indicated otherwise in a credit line to the material. If material is not included in the article's Creative Commons licence and your intended use is not permitted by statutory regulation or exceeds the permitted use, you will need to obtain permission directly from the copyright holder. To view a copy of this licence, visit <http://creativecommons.org/licenses/by/4.0/>. The Creative Commons Public Domain Dedication waiver (<http://creativecommons.org/publicdomain/zero/1.0/>) applies to the data made available in this article, unless otherwise stated in a credit line to the data.

identified the majority of the intermediate NFT score subjects in an autopsy-confirmed study. As far as we know, this is the first study that presents a visualization of ante-mortem FTP retention patterns that at a group level agree with the neurofibrillary tangle staging scheme proposed by Braak. These findings suggest that the *Et* VOI may be sensitive for detecting impaired subjects early in the course of Alzheimer's disease.

Key points

- Question: Can a flortaucipir VOI made up of temporal lobe structures (*Et* VOI) identify patients early in the course of AD?
- Pertinent findings: The *Et* VOI identified subjects with elevated temporal, but not global flortaucipir PET signal who were primarily A β +, *APOE* ϵ 4 carriers, and diagnosed as MCI or AD. The identified patients demonstrated modest tau accumulation, neurodegeneration, and cognitive decline within 18 months. Finally, the *Et* VOI identified the majority of the amyloid-positive, Braak IV (intermediate ADNC score) subjects in an autopsy-confirmed study.
- Implications for patient care: In research settings, the early tau VOI might aid in the identification and stratification of patients early in the course of AD who may derive maximal benefit from therapeutic intervention.

Introduction

The defining neuropathological hallmarks of Alzheimer's disease (AD) are an extracellular accumulation of aggregated amyloid- β fragments, typically associated with degenerating neurites (amyloid- β neuritic plaques), and intracellular aggregates of abnormally phosphorylated microtubule-associated tau protein (neurofibrillary tangles [NFTs]) [1, 2]. NFTs may be found within the transentorhinal cortex and nearby mesial temporal lobe structures of both healthy older adults and subjects with Alzheimer's disease dementia [3]. However, the widespread presence of NFTs in the neocortex is typically associated with cognitive impairment [4]. It is hypothesized that in individuals on the Alzheimer's disease pathway, amyloid plaques (A β) trigger the spread of neurofibrillary tangles beyond the transentorhinal cortex [5, 6].

With the advancement of positron emission tomography (PET) imaging biomarkers for amyloid (the approved agents florbetapir F 18, florbetaben F 18, and flutemetamol F 18) and tau (the approved agent flortaucipir F 18 as well as experimental agents such as ¹⁸F-MK-6240 and ¹⁸F-PI-2620), the density and distribution of misfolded amyloid beta and hyperphosphorylated tau aggregates can be estimated in vivo [7–12]. Fleisher

et al. [13] have recently shown in an autopsy-confirmed dataset that a specific pattern of flortaucipir neocortical retention was associated with both Braak V/VI stage or B3 NFT score and A β accumulation, which is consistent with high AD neuropathological change according to the NIA-AA criteria [4, 14].

Recent studies have also shown a correlation between flortaucipir estimation of tau burden and increasing progression of cognitive impairment even when the analysis is limited to amyloid-positive subjects [15–17]. These findings suggest that moderate to advanced tau burden as estimated by flortaucipir might help confirm AD diagnosis and identify patients most likely to deteriorate within a subsequent 18-month time period.

In addition to confirming the presence of AD pathology, there has been increasing interest in utilizing tau PET imaging to identify patients at the earliest stages of AD [18–20]. Braak et al. have suggested that tau starts in the transentorhinal cortex, spreads to the entorhinal cortex, and then extends into the fusiform and temporal gyri before spreading to the parietal, occipital, and frontal cortices [21, 22]. Multiple neuropathological studies report on the presence of NFTs in the medial temporal lobes of cognitively normal subjects [3, 23, 24]. Increased tracer retention has been shown in the temporal regions of cognitively normal, amyloid-positive, and amyloid-negative subjects using tau PET imaging [17, 19, 25]. Composite temporal volumes-of-interest (VOIs) to quantify early AD subjects from tau PET images have been previously proposed [26–29]. In this work, we hypothesized that a similar temporal composite VOI for flortaucipir imaging comprising medial/ inferior temporal lobe structures might identify subjects that may be in the earliest stages of AD tauopathy before widespread tau accumulation. We applied this VOI in two longitudinal clinical trials, as well as a separate autopsy validation study to identify subjects with tau limited to the temporal regions. For the two longitudinal studies, we also examined the changes in tau accumulation, neurodegeneration, and cognition over 18 months associated with baseline temporal VOI findings. The main goal of our work was the identification and disease progression of early tau subjects that might not have global tau uptake. In the autopsy-confirmed dataset, we evaluated the sensitivity of the VOI for identifying intermediate Braak stage pathology.

Methods

Subjects

Longitudinal study 1 and study 2 (18-F-AV1451-A05 exploratory and Expedition 3)

We retrospectively analyzed 427 subjects from our exploratory longitudinal study of flortaucipir (A05-exploratory, NCT02016560) and a previously completed therapeutic trial where flortaucipir was used as a biomarker (Expedition 3/ NCT01900665). In both trials, subjects received flortaucipir, florbetapir, anatomical magnetic resonance imaging (T₁-weighted MRI), and a battery of cognitive assessments both at baseline and approximately at 18 months. Some of the Expedition 3 trial participants received solanezumab as treatment; all the A05 subjects were untreated. None of the participants received solanezumab treatment prior to baseline flortaucipir or florbetapir scans. The demographics of all these subjects are shown in Table 1.

Study 3 (18-F-AV1451-A16)

Sixty-seven subjects with a terminal illness, a projected life expectancy of less than 6 months, and older than 50 years underwent ante-mortem flortaucipir PET imaging [13]. These subjects were then followed with brain autopsy (18-F-AV1451-A16, NCT02516046). Two pathologists blinded to the clinical and imaging results recorded neuropathological findings according to the NIA-AA guidelines [4, 14]. Braak pathological staging of NFTs was performed by AT8 monoclonal antibody, and Aβ plaques were detected using 6E10 Aβ₁₋₄₂ monoclonal antibody using immunohistochemical staining methods [13]. The demographics of these subjects are shown in Table 2.

Image acquisition

Study 1 (NCT02016560/18-F-AV1451-A05 exploratory)

Flortaucipir images were acquired for 20 min (4 × 5 minute frames) from 80 to 100 min post-injection of approximately 370 MBq (10mCi) of flortaucipir F 18.

On a separate day, 10-min florbetapir images were acquired between 50 and 60 min post-injection of approximately 370 MBq (10mCi) of florbetapir F 18. PET data were reconstructed using scanner-specific iterative reconstruction algorithms (FORE, OSEM, or RAMLA) with 3–6 iterations, 16–33 subsets, and post-smoothing of 3–5 mm (or “normal” or “sharp” settings).

Each subject also underwent a 3D T₁-weighted MRI scan on either a 1.5-T or 3-T scanner. The MRI protocol included sagittal 3D MPRAGE (Siemens), sagittal 3D T1-TFE (Philips), or sagittal 3D IR-FSPGR (GE) sequences with 1.2-mm-thick slices (no gap) and 0.9375–1.25 × 0.9375–1.25 mm² in-plane resolution.

Study 2 (NCT01900665/Expedition 3)

Flortaucipir images were acquired for 30 min (6 × 5 minute frames) from 75 to 105 min post-injection of 240 MBq (6.5 mCi) of flortaucipir F 18. The reconstruction algorithms were similar to study 1. All subjects also underwent florbetapir PET scans 50–70 min after injection of 370 MBq florbetapir F 18 and were required to be amyloid-positive by visual interpretation of PET at screening. The MRI acquisition parameters were the same as in study 1.

Study 3 (NCT02516046/18-F-AV1451-A16)

For this autopsy study in end-of-life patients, flortaucipir acquisition parameters were the same as in study 1. No florbetapir or MRI data were acquired. Amyloid positivity was determined by a CERAD score of moderate to frequent at autopsy.

Image processing and interpretation

Florbetapir (A05E)

For each subject, the florbetapir PET frames were motion-corrected (MCFLIRT [30]) and averaged to

Table 1 Demographics of subjects that were retrospectively analyzed in this work. Age is represented as mean ± standard deviation. MMSE is also represented as mean ± standard deviation. All the 109 subjects who received solanezumab were amyloid-positive and mild to moderate AD cases. YCN young cognitively normal, CN cognitively normal, MCI mild cognitive impairment, AD Alzheimer's disease, N number of subjects, MMSE Mini-Mental State Examination, F female, M male. CD college degree or higher, HS high school or lower, C Caucasian, NC Not Caucasian (Asian, Black or African American, Other)

	YCN/Aβ-	CN/Aβ-	CN/Aβ+	MCI/Aβ-	MCI/Aβ+	AD/Aβ-	AD/Aβ+
N	16	53	5	50	47	16	240
Age	28.9 ± 4.9	67.6 ± 10.2	77.8 ± 7.0	69.1 ± 9.3	72.7 ± 9.1	72.2 ± 6.9	73.7 ± 8.3
MMSE	29.6 ± 0.5	29.5 ± 0.5	29.6 ± 0.5	28.2 ± 1.7	27.4 ± 1.8	22.9 ± 3.2	22.5 ± 2.9
Sex	7F/9M	24F/29M	2F/3M	27F/23M	21F/26M	7F/9M	135F/104M
Education	15CD/1HS	45CD/8HS	4CD/1HS	37CD/13HS	38CD/9HS	14CD/2HS	141CD/97HS
Race	11C/5NC	42C/11NC	5C/0NC	43C/7NC	45C/2NC	14C/2NC	192C/22NC

Table 2 Demographics of the autopsy-confirmed subjects, where *N* is the number of subjects, age is represented as mean \pm SD, and gender is shown as female/male. *CD* college degree or higher, *HS* high school or lower, *C* Caucasian, *NC* Not Caucasian (Asian, Black or African American, Other)

	B1		B2		B3	
	Braak I	Braak II	Braak III	Braak IV	Braak V	Braak VI
N	2	5	4	11	14	24
Age	67 \pm 1.7	76.8 \pm 6.8	85.8 \pm 10.4	86.8 \pm 6.3	85.6 \pm 8.5	81.7 \pm 9.4
Sex	1F/ 1M	3F/ 2M	3F/ 1M	6F/ 5M	5F/ 9M	15F/ 9M
Education	1CD/1HS	2CD/3HS	3CD/1HS	4CD/7HS	11CD/3HS	14CD/10HS
Race	2C/0NC	4C/1NC	4C/0NC	11C/0NC	14C/0NC	24C/0NC

create a single static image. Flortetapir static images were spatially aligned to the Montreal Neurological Institute (MNI) template and normalized using the whole brain cerebellum to create an SUVR image [31]. The average SUVR from six predefined ROIs was calculated. Visual assessment of the flortetapir images supplemented by SUVR was used to determine A β positivity [32].

Flortetapir (studies 1 and 2)

Dynamic flortetapir PET frames were corrected for inter-frame motion (McFLIRT [30]) and acquisition start time deviations prior to averaging to create a static image. The mean PET static baseline flortetapir image for a given subject was rigidly aligned to the subject's baseline MRI. Follow-up flortetapir images were aligned to the baseline PET. A nonlinear transformation of the subject's baseline MRI to the MNI template was conducted. This non-linear transformation was applied to the native space-aligned flortetapir PET images from all time points. A subject-specific, data-driven, white matter reference region (PERSI) [33] was used for count normalization. In addition to PERSI, we evaluated the performance of previously published cerebellum crustaneous as a reference region. We excluded 37 subjects from further analyses due to severe motion that affected quantitation and image artifacts or difficulties identifying a separable white matter peak for the reference region that led to failures in quantification.

Flortetapir (study 3)

Dynamic flortetapir images from study 3 were corrected for motion and acquisition start time deviations prior to creating static images, similar to studies 1 and 2. Since subjects in this study did not receive an MRI, the PET image was directly aligned to a flortetapir PET template. This flortetapir PET template was created by averaging previously aligned MNI space flortetapir PET

images from study 1. Seven subjects from this study were excluded from further analyses due to image artifacts or severe motion.

Visual interpretation

Flortetapir images from all three studies were visually read by imaging physicians as either not consistent with AD (negative AD tau pattern/ τ AD $-$) or consistent with AD (moderate/ τ AD $+$, or advanced/ τ AD $++$ tau pattern), based on neocortical tracer pattern [34].

Analysis

Early tau VOI

Based on preliminary analyses performed to separate A β $+$ controls from A β $-$ controls and evidence in the literature of early involvement of temporal lobe structures in tau accumulation [19, 25, 26, 28, 35], we selected entorhinal cortex, parahippocampal, fusiform, and inferior temporal gyri to create an "early tau" VOI ($E\tau$ VOI) to capture what we hypothesize would be the region of early flortetapir uptake. We transformed the FreeSurfer [36] FsAverage template to the MNI space and extracted the volumes based on the Desikan-Killiany atlas [37] to create the VOI. Figure 1A is a surface representation of the $E\tau$ VOI. Figure 1B is the volumetric representation of the $E\tau$ VOI, which was applied to all the subjects.

AD signature-weighted neocortical VOI for the estimation of global tau burden

In order to estimate the global tau burden, we used a data-driven volume of interest that was designed to maximize separation between diagnostic groups (A β $+$ AD, A β $+$ mild cognitive impairment [MCI] vs dementia, MCI, and cognitive normal [CN] A β $-$ subjects) using a multiblock barycentric discriminant analysis (MUBADA) [38]. As shown in Fig. 1C, the AD signature-weighted neocortical VOI ($AD_{signature}$) [39] has higher weights in the posterolateral temporal and parietal regions.

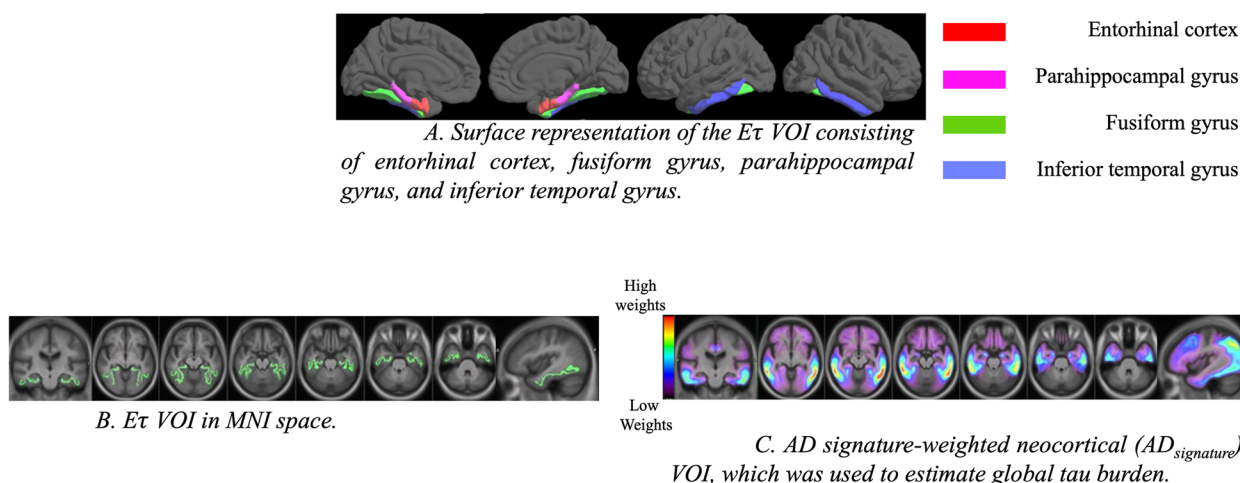


Fig. 1 **A** Surface representation of the Et VOI consisting of the entorhinal cortex, fusiform gyrus, parahippocampal gyrus, and inferior temporal gyrus. **B** Et VOI in MNI space. **C** AD signature-weighted neocortical ($AD_{signature}$) VOI, which was used to estimate global tau burden

SUVr analysis and subject grouping

The Et VOI and $AD_{signature}$ VOI SUVRs were calculated relative to a white matter reference region (PERSI) [33]. Sixteen cognitively normal, young (age = 28.9 ± 4.9) subjects from study 1 were used to determine SUVr thresholds for positivity for each volume of interest. Thresholds for positivity were defined as the mean + 2.5 times standard deviation of SUVRs from these sixteen young controls. Based on SUVr thresholds within the Et VOI (1.1052) and $AD_{signature}$ VOI (1.1059), subjects were divided into quadrants of elevated or low tau signal (Fig. 2). Subjects

elevated in both Et and $AD_{signature}$ VOIs were represented as $Et+/AD_{signature}+$, subjects positive for Et alone were $Et+/AD_{signature}-$, subjects with low Et and $AD_{signature}$ were $Et-/AD_{signature}-$, and subjects with low Et and high $AD_{signature}$ were $Et-/AD_{signature}+$. Since only two subjects were $Et-/AD_{signature}+$, we did not include them in any analysis. Among these groups, we were particularly interested in $Et+/AD_{signature}-$ subjects as this sub-group represented subjects with tau uptake primarily restricted to the regional Et VOI, but below the threshold for the global AD signature-weighted neocortical VOI.

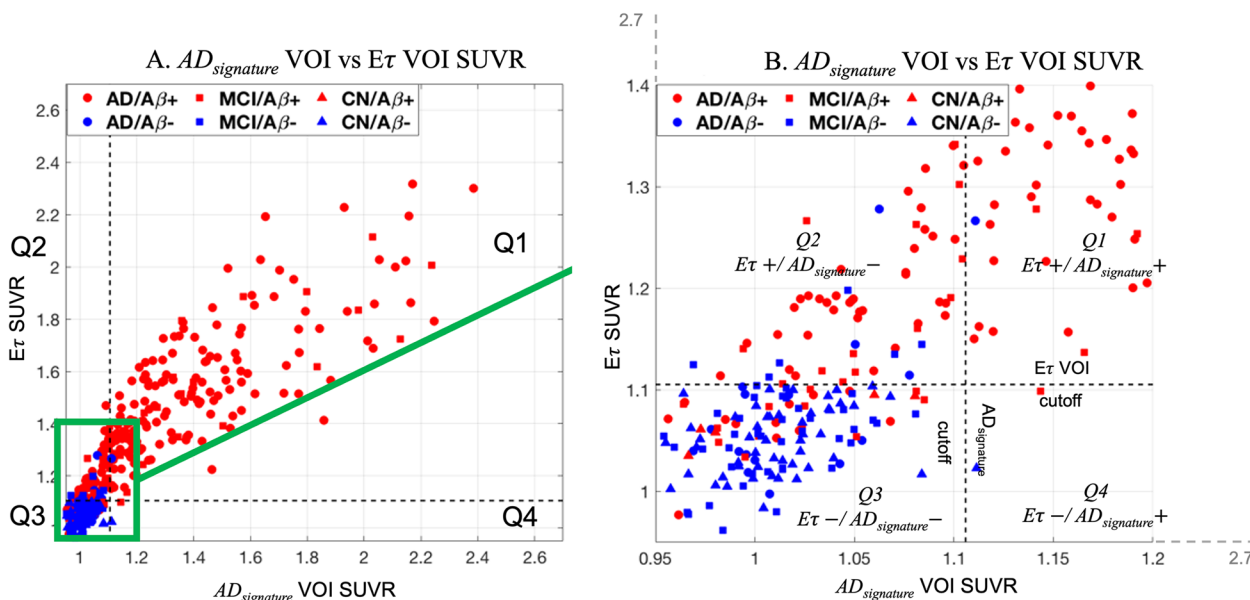


Fig. 2 **A** Scatter plot showing $AD_{signature}$ SUVr vs Et VOI SUVr with subjects color-coded based on amyloid status ($A\beta+$ is red and $A\beta-$ is blue). **B** A zoomed sub-section of **A** highlighting the subjects in the $Et+/AD_{signature}-$ quadrant

Cortical thickness

Each subject's baseline and 18-month T_1 -weighted MRI was processed in FreeSurfer version 5.3 [36] to generate subject-specific regional cortical thickness measures. Subjects with image or motion artifacts in MRI were excluded from cortical thickness assessments. Since we do not expect tau uptake in $E\tau$ VOI to impact neurodegeneration outside of the early tau region, we calculated vertex-weighted average thickness from the $E\tau$ VOI regions (entorhinal cortex, fusiform, parahippocampal, and inferior temporal gyri) using the Desikan-Killiany atlas for each subject. We calculated the difference in thickness between the two time points within the $E\tau$ VOI regions to capture cortical thinning.

Statistical analysis

To understand whether subjects with elevated $E\tau$ VOI (temporal) signal and low AD signature-weighted neocortical VOI (global) signal, i.e., $E\tau+/AD_{signature-}$ subjects, were likely to progress, we performed quadrant-wise statistical analyses. Subjects that were $E\tau+/AD_{signature+}$, $E\tau+/AD_{signature-}$, and $E\tau-/AD_{signature-}$ were compared for tau accumulation in $E\tau$ and $AD_{signature}$ VOI, cortical atrophy within $E\tau$ regions, and cognition. To eliminate any treatment-related confounds, we excluded 109 subjects from Expedition 3 trial that received solanezumab from all longitudinal statistical analyses.

We calculated the baseline and 18-month change in $E\tau$ VOI SUVR and AD signature-weighted neocortical SUVR for each subject to assess tau accumulation. The Kruskal-Wallis test was performed to assess the group differences across quadrants. Post hoc tests were performed between each of the three quadrants. Similar to the change in tau accumulation, we performed group comparisons and post hoc analyses for baseline cortical thickness and 18-month change in thickness.

For evaluating cognitive decline, we compared the 18-month change in Mini-Mental State Examination (MMSE) across quadrants. We also compared the 18-month change in Pfeffer Functional Activities Questionnaire (FAQ) and Alzheimer's Disease Assessment Scale 11-item Cognitive Subscale (ADAS-Cog11).

Validation in autopsy data

The $E\tau$ and AD signature-weighted neocortical VOI SUVRs were also derived for subjects in study 3. Scatter plots of the autopsy-confirmed Braak stage against the SUVR were used to assess the number of subjects in each Braak stage above the cutoffs for $E\tau$ and $AD_{signature}$ VOIs.

Neocortical flortaucipir uptake

In order to explore whether the $E\tau+/AD_{signature-}$ subjects have elevated tau uptake in other regions besides the $E\tau$ VOI, we created quadrant-wise average surface maps for each of the three quadrants. Each quadrant's average image was projected onto the FsAverage surface.

Voxel-wise z -scores were determined for each subject relative to SUVR values from the sixteen young controls from study 1. For each voxel, group-wise average z -scores were measured by grouping subjects within the previously identified quadrants $E\tau+/AD_{signature+}$, $E\tau+/AD_{signature-}$, and $E\tau-/AD_{signature-}$. If the average z -score of a voxel was at least 2, it was considered as being tau positive. In order to observe if tau positivity in a voxel was present in multiple subjects, we also calculated the percentage of tau-positive (z -score > 2) subjects within each voxel.

The same approach was applied to study 3 (autopsy-confirmed dataset) to create average surface maps based on NFT scores.

Results

Subject distribution

Of all the baseline subjects in this study, 171 subjects showed elevated signal in both $E\tau$ VOI and $AD_{signature}$ VOI ($E\tau+/AD_{signature+}$), 64 subjects were identified as having elevated $E\tau$ VOI signal in the absence of $AD_{signature}$ VOI signal ($E\tau+/AD_{signature-}$), 153 subjects had low signal on both $E\tau$ and $AD_{signature}$ VOI ($E\tau-/AD_{signature-}$), and 2 subjects were high on $AD_{signature}$ and low on $E\tau$ VOI ($E\tau-/AD_{signature+}$) (Fig. 2A, B). $E\tau+/AD_{signature+}$ subjects were 99% $A\beta+$, 100% diagnosed as either AD (88%) or MCI (12%), and 74% were $APOE \epsilon 4$ carriers. $E\tau+/AD_{signature-}$ subjects were 84% $A\beta+$, 100% were either AD (67%) or MCI (33%), and 59% were $APOE \epsilon 4$ carriers. In contrast, $E\tau-/AD_{signature-}$ subjects were only 19% $A\beta+$, 18% AD (40% MCI), and 30% $APOE \epsilon 4$ carriers. Since all subjects in study 2 were $A\beta+$ and mild to moderate AD, we also calculated percentages in study 1. We observed that 98% of subjects in $E\tau+/AD_{signature+}$, 68% of subjects in $E\tau+/AD_{signature-}$, and 13% of subjects in $E\tau-/AD_{signature-}$ were $A\beta+$ in study 1. In terms of $APOE \epsilon 4$ carrier status, 73% of $E\tau+/AD_{signature+}$ subjects, 50% of $E\tau+/AD_{signature-}$ subjects, and 29% of $E\tau-/AD_{signature-}$ subjects were $APOE \epsilon 4$ carriers. These results are shown in Additional file 5: Table S1.

SUVR, thickness, and cognition/function

There was a significant difference in baseline flortaucipir SUVR between $E\tau+/AD_{signature+}$, $E\tau+/AD_{signature-}$, and $E\tau-/AD_{signature-}$ for both $E\tau$ and $AD_{signature}$ VOIs (Fig. S1). Elevation in flortaucipir retention in the $E\tau$ VOI had consequences for future changes in SUVR and cortical thickness in the early tau region,

as well as for cognitive deterioration. Compared to $Et\tau-/AD_{signature-}$ subjects, $Et\tau+/AD_{signature-}$ and $Et\tau+/AD_{signature+}$ had significantly greater SUVR increases over 18 months in both $Et\tau$ (Fig. 3A) and $AD_{signature}$ (Fig. 3B) regions. $Et\tau+/AD_{signature+}$ subjects had greater SUVR increases than $Et\tau+/AD_{signature-}$ subjects in the $AD_{signature}$ VOI (Fig. 3B). However, for the $Et\tau$ VOI, there was no difference in SUVR increase between the $Et\tau+/AD_{signature-}$ and $Et\tau+/AD_{signature+}$ subjects (Fig. 3A).

Similar differences were seen for the changes in cortical thickness within the $Et\tau$ VOI (Fig. 3C), among the three quadrants. Likewise, significant differences were observed between all quadrants for 18-month change in MMSE (Fig. 3D). There was also a significant difference between $Et\tau-/AD_{signature-}$ and $Et\tau+/AD_{signature-}$ or $Et\tau+/AD_{signature+}$ subjects for 18-month change in ADAS-Cog11 and FAQ. However, differences in the change from baseline ADAS-Cog11 or FAQ between $Et\tau+/AD_{signature-}$ and $Et\tau+/AD_{signature+}$ subjects did not reach statistical significance.

We observed that using the cerebellum crustaneous reference region resulted in fewer subjects being identified as $Et\tau+/AD_{signature-}$. While the subjects identified using cerebellum crustaneous had on average greater tau accumulation, larger cortical thinning, and higher cognitive decline in 18 months, they were not significantly different from $Et\tau-/AD_{signature-}$ group (Fig. S2A-D).

Validation in autopsy-confirmed dataset

In the autopsy-confirmed data, 32 of the 38 B3 NFT score subjects had elevated $AD_{signature}$ VOI signal (Fig. 4A), and 30/38 B3 NFT score subjects had elevated

$Et\tau$ VOI signal (Fig. 4B) as seen in the scatter plots (Fig. 4A, B). In contrast, none of the 15 B2 NFT score subjects had elevated $AD_{signature}$ VOI signal, but 12/15 (including 10/11 Braak IV) had elevated $Et\tau$ VOI signal (Fig. 4B). None of the B1 NFT score subjects had elevated $AD_{signature}$ VOI signal, one B1 (Braak II) NFT score subject had elevated $Et\tau$ VOI signal.

With cerebellum crustaneous reference region, 31/38 B3 NFT score subjects had elevated $AD_{signature}$ and $Et\tau$ VOI signal. Three of the 15 B2 NFT score subjects had elevated $AD_{signature}$ signal but 7/15 B2 NFT score subjects had elevated $Et\tau$ VOI signal. None of the B1 NFT score subjects had elevated $AD_{signature}$ VOI signal, while one B1 (Braak II) NFT score subject had an elevated $Et\tau$ VOI signal (Fig. S3A, B).

Neocortical tau burden

There were no vertices of elevated flortaucipir uptake in $Et\tau-/AD_{signature-}$ subjects (Fig. 5A). For $Et\tau+/AD_{signature-}$ subjects, as hypothesized, elevated uptake was primarily restricted to the $Et\tau$ VOI, with the exception of left middle temporal gyrus (Fig. 5B). $Et\tau+/AD_{signature+}$ subjects had elevated uptake across the entire cortex sparing the precentral, postcentral, and paracentral gyri and the anterior cingulate (Fig. 5C).

Figure 5D-F shows the percentage of subjects with regional tau positivity for $Et\tau-/AD_{signature-}$, $Et\tau+/AD_{signature-}$, and $Et\tau+/AD_{signature+}$, respectively. None of the $Et\tau-/AD_{signature-}$ subjects were tau-positive in any of the regions sampled at the selected threshold. Within the $Et\tau$ VOI, 70% of $Et\tau+/AD_{signature-}$ subjects were tau-positive, with 90.7% positive in the left entorhinal cortex, 87.5%

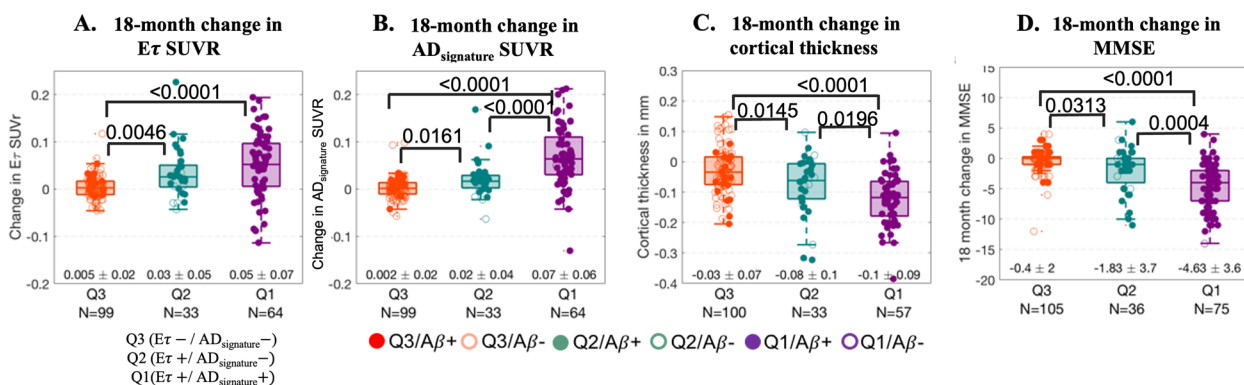


Fig. 3 A Boxplots showing the 18-month change in $Et\tau$ VOI SUVR across the quadrants. The 18-month change in $Et\tau$ VOI SUVR was significantly different between subjects in Q2 (or Q1) and Q3. **B** Boxplots showing the 18-month change in $AD_{signature}$ VOI SUVR across the quadrants. The 18-month change in $AD_{signature}$ VOI SUVR was significantly different across the quadrants (Q1 > Q2 > Q3). **C** Boxplots showing the 18-month change in cortical thickness across the quadrants. The 18-month change in cortical thickness was significantly different across the quadrants (Q1 < Q2 < Q3). **D** Boxplot showing the 18-month change in MMSE across the quadrants. The 18-month change in MMSE was significantly different across quadrants (Q1 < Q2 < Q3). A total of 109 subjects from the treatment arm of the solanezumab trial were excluded from these analyses. Note: the N's are different in the above boxplots for flortaucipir change, thickness, and MMSE due to the availability of the data

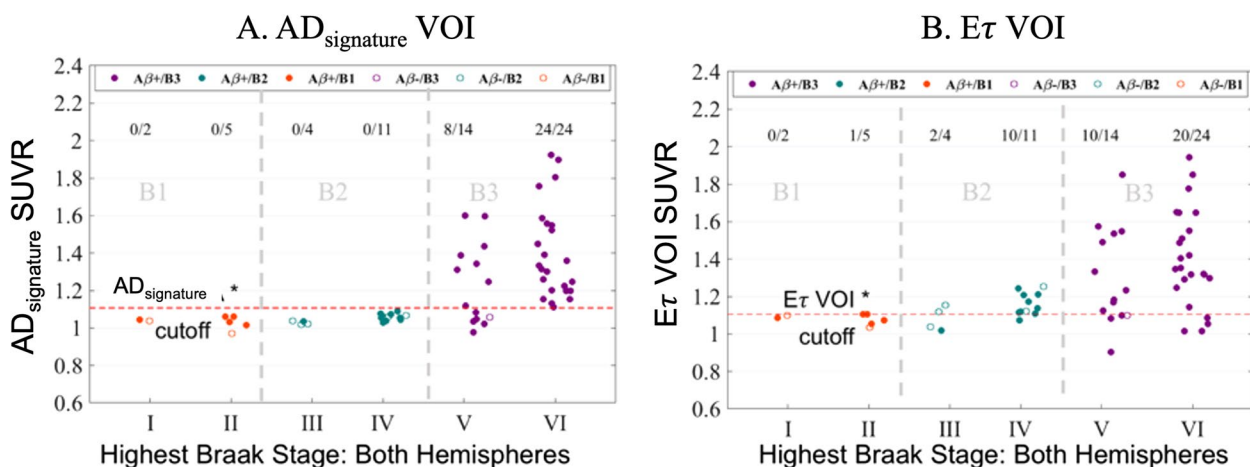


Fig. 4 **A** Scatter plot of Braak stage vs AD_{signature} VOI SUVR. The red dotted line represents the AD_{signature} positivity cutoff of 1.1059. The numbers at the top represent the number of subjects for each Braak stage. For example, for Braak VI, 24/24 indicates that of the 24 Braak VI subjects in this analysis, 24 had elevated AD_{signature} signals. **B** Scatter plot of Braak stage vs Et τ VOI SUVR. The red dotted line represents the Et τ VOI SUVR positivity cutoff of 1.1052. Amyloid positivity is defined by a CERAD score of moderate to frequent at autopsy

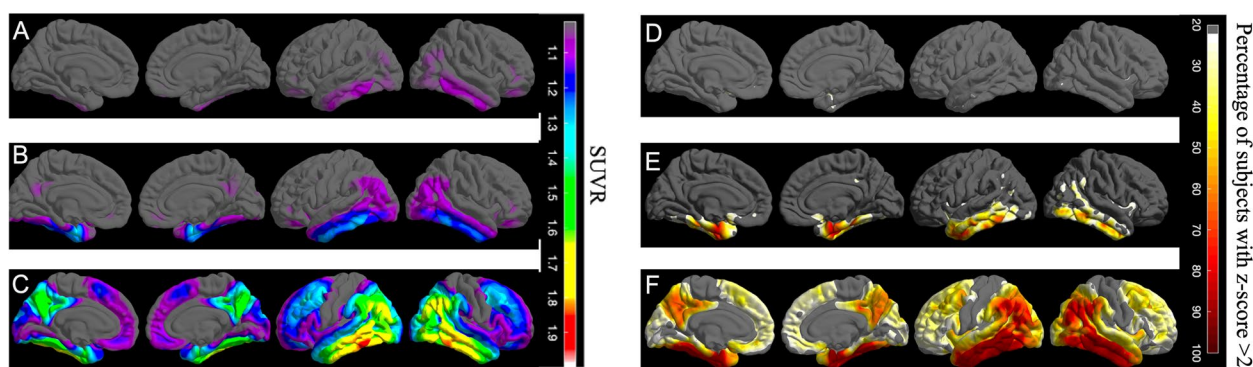


Fig. 5 **A** The average SUVR surface map of Q3 (Et-/AD_{signature}-) subjects, showing a lack of elevated flortaucipir signal in the entire cortex. **B** The average SUVR surface map of Q2 (Et+/AD_{signature}-) subjects. There is an elevated flortaucipir signal primarily in the regions of Et τ VOI region with the exception of the left middle temporal gyrus. **C** The average SUVR surface map of Q1 (Et+/AD_{signature}+) subjects. Widespread elevation of flortaucipir signal across the entire cortex with the exception of postcentral, precentral, and paracentral gyri and anterior cingulate. **D-F** Surface maps showing the percentages of subjects that are tau positive for all FreeSurfer regions in Q3 (Et-/AD_{signature}-), Q2 (Et+/AD_{signature}-), and Q1 (Et+/AD_{signature}+), respectively

in the right entorhinal cortex, 92.2% in the left inferior temporal gyrus, and 67.2% in the right inferior temporal gyrus. Within the neo-cortex, outside the Et τ VOI, 46.8% of subjects in Et τ +/AD_{signature}- were positive in the left middle temporal gyrus, 35.9% in the right middle temporal gyrus, and only 28.1% in the right inferior parietal gyrus. For Et τ +/AD_{signature}+ subjects, the percentage of tau positivity was highest (~ 90%) within the medial/lateral temporal including the Et τ VOI and inferior parietal structures, followed by superior temporal, superior parietal, and supramarginal regions (~ 60%) and frontal regions (~ 50%).

Similar to surface maps of studies 1 and 2, we observed that there were no regions of elevated flortaucipir uptake in B1 NFT score subjects (Fig. 6A). The elevated uptake was primarily restricted to the Et τ VOI, with the exception of bilateral parahippocampal gyrus for B2 NFT score subjects. There was an elevation in the middle temporal gyrus, sections of the medial orbitofrontal gyrus, and anterior cingulate for B2 NFT score subjects (Fig. 6B). We observed elevated uptake across the entire cortex sparing the precentral, post-central, and paracentral gyri and the anterior cingulate for B3 NFT score subjects (Fig. 6C). Voxel-wise z-score

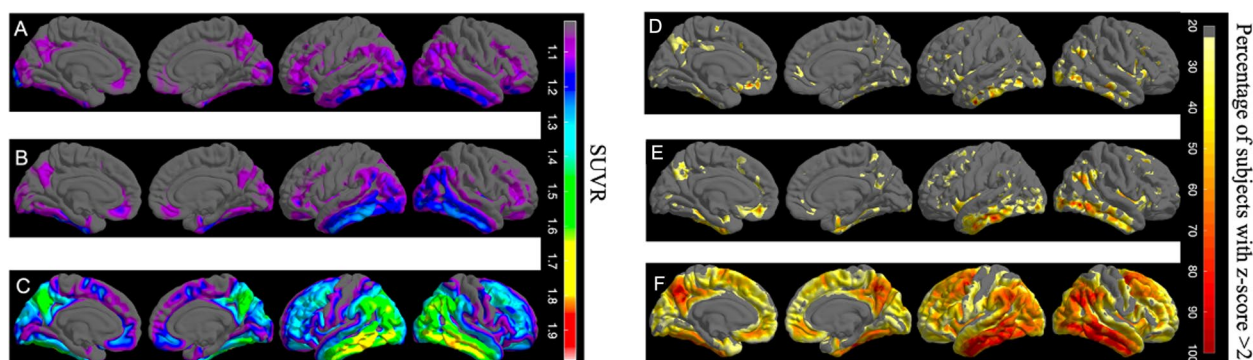


Fig. 6 **A** The average SUVR surface map of B1 subjects, showing a lack of elevated flortaucipir signal in the entire cortex. **B** The average SUVR surface map of B2 subjects. There is an elevated flortaucipir signal primarily in the regions of *E τ* VOI region with the exception of the left middle temporal gyrus. **C** The average SUVR surface map of B3 subjects. Widespread elevation in flortaucipir signal across the entire cortex with the exception of postcentral, precentral, and paracentral gyri and anterior cingulate. **D** Surface map showing the percentages of subjects that are tau-positive for all FreeSurfer regions in B1. **E** Surface map showing the percentages of subjects that are tau-positive for all FreeSurfer regions in B2. **F** Surface map showing the percentages of subjects that are tau-positive for all FreeSurfer regions in B3

surface maps yielded a similar pattern of elevated uptake (Fig. 6D–F).

Discussion

In this study, we identified a population of patients with elevated flortaucipir signal in the early tau region (*E τ* VOI) and low global AD signature-weighted neocortical VOI uptake. The subjects with elevated *E τ* VOI signal and low AD signature-weighted neocortical VOI signal were 84% A β +, 59% *APOE* ϵ 4 carriers, and diagnosed as MCI or AD. (Fig. 2).

The quadrant-wise statistical analysis disclosed significantly different 18-month tau accumulation between *E τ* -/*AD*_{signature}- subjects compared to *E τ* +/*AD*_{signature}- for both *AD*_{signature} and *E τ* VOIs (Fig. 3A, B). While there was a significant difference between subjects in *E τ* +/*AD*_{signature}- and *E τ* +/*AD*_{signature}+ for *AD*_{signature} SUVR, we did not observe a significant difference in 18-month *E τ* VOI accumulation. *E τ* +/*AD*_{signature}- subjects had 18-month change in thickness values in-between *E τ* -/*AD*_{signature}- and *E τ* +/*AD*_{signature}+ (Fig. 3C). Furthermore, the 18-month change in MMSE (Fig. 3D), ADAS-Cog11, and FAQ values for *E τ* +/*AD*_{signature}- subjects were between *E τ* +/*AD*_{signature}+ and *E τ* -/*AD*_{signature}-, suggesting that *E τ* +/*AD*_{signature}- subjects may be intermediate stage subjects. These findings also suggest that *E τ* +/*AD*_{signature}- subjects might be at an earlier stage of AD pathology relative to *E τ* +/*AD*_{signature}+ subjects.

The performance of the *E τ* VOI in identifying early-stage subjects was explored in the autopsy-confirmed cohort. We observed that 80% (12/15) of B2 pathology subjects, including 10/11 Braak IV cases, had an elevated *E τ* SUVR in the absence of an elevated AD signature-weighted neocortical SUVR. In contrast, only 2/4 Braak

III subjects had elevated *E τ* VOI signal. While there was increased sensitivity in the detection of B2 pathology subjects using the *E τ* VOI, 4 Braak VI subjects were misclassified as having no *E τ* flortaucipir uptake. Similarly, 4 Braak V subjects were also misclassified. We suspect this might be due to the significant atrophy in these subjects, particularly within the early tau regions. It is widely reported that medial temporal regions are likely to be atrophied first in AD [40, 41]. Accordingly, the SUVR in these early tau regions might be lower compared to further downstream tau regions such as posterolateral temporal and parietal, which is where *AD*_{signature} mainly samples from. Although a small sample, this might suggest that the *E τ* VOI, when compared to the *AD*_{signature} VOI, was sensitive at identifying Braak IV cases (Fig. 4B). While previous neuropathologic studies have demonstrated the correlation between neurofibrillary tangles and flortaucipir retention [42, 43], studies on flortaucipir PET images with autopsy confirmation in moderate sample sizes are limited. Accordingly, one strength of the current work is the identification of a positive signal with the *E τ* VOI in a moderate sample of autopsy-confirmed intermediate Braak pathology subjects.

Our data suggests that PERSI might provide better sensitivity in identifying subjects that progress within 18 months. While the trends with cerebellum crustaneous were similar to the PERSI reference region, tau accumulation and cortical thinning were not significantly different between *E τ* -/*AD*_{signature}- and *E τ* +/*AD*_{signature}- groups. As previously published, the PERSI reference region had lesser variability in SUVR of controls compared to cerebellum crustaneous [33]. This increased variability necessitates a higher cutoff for *E τ* VOI with cerebellum crustaneous reference region to provide the same

confidence in the identification of elevated signal resulting in fewer subjects being identified as $E\tau+/AD_{signature-}$.

$E\tau+/AD_{signature-}$ subjects were defined by elevation in $E\tau$ VOI but not in $AD_{signature}$. In order to determine whether there might be other regions also affected in $E\tau+/AD_{signature-}$ subjects, we sampled the entire cortex and created surface maps. Based on the surface maps (Fig. 5B, E), the involvement of medial structures such as the entorhinal cortex, fusiform, and parahippocampal gyri and a lateral structure (inferior temporal gyrus) was evident across the majority of $E\tau+/AD_{signature-}$ subjects. Widespread involvement of multiple regions was seen in $E\tau+/AD_{signature+}$ subjects (Fig. 5C, F) with the absence of flortaucipir signal across the entire cortex for $E\tau-/AD_{signature-}$ subjects (Fig. 5A, D). The surface maps of the autopsy data showed similar findings, where the involvement of the entorhinal cortex, fusiform, parahippocampal, and inferior temporal gyrus was evident across the majority of B2 NFT score subjects. B2 NFT score subjects also showed elevated flortaucipir uptake in the sections of the medial orbitofrontal region and anterior cingulate gyrus (Fig. 6B, E). The pattern of elevation of flortaucipir retention was consistent with neuropathological Braak stage and with the proposed sensitivity of the $E\tau$ region to B2 pathology.

This work has several limitations. Since not all participants with PET data have MRIs, particularly our autopsy study participants, we created a template space VOI. As the VOI is a template-based region, which is derived from anatomical MRI, it is relatively small and restricted to the cortex. Consequently, uptake might be reduced in cases of substantial temporal lobe atrophy or instances of misalignments to the MNI template. Subjects with high levels of tau and atrophy might lead to difficulties in quantification. The majority of the 8.7% (37/427) subjects excluded in this analysis have either high levels of tau or atrophy. Since we are primarily interested in subjects with early stages of tau accumulation, we believe the exclusion of these subjects does not affect our findings. Here, we used a data-driven $AD_{signature}$ VOI to represent global tau uptake and a template-based $E\tau$ VOI to characterize regional tau uptake. Not including a data-driven version of the early tau VOI might be another limitation of this work, however, some reports suggest similar spatial distribution patterns between data-driven and anatomical VOIs, particularly in early tau regions [29]. Furthermore, data-driven VOIs can rely heavily on the datasets used to develop them and may not be easily generalizable to other datasets.

Another limitation of the approach in this study is the inclusion of older $A\beta-$ controls. While one might argue that the statistical difference observed is driven by the controls, it is important to note that the subjects were

classified into quadrants agnostic to their clinical diagnosis or amyloid status. Furthermore, subject grouping based on the $E\tau$ VOI may be sensitive to classifying controls as being tau negative.

The small number of $A\beta+$ cognitively normal subjects in our cohort is another limitation of our study. The prevalence of AD or MCI subjects in $E\tau+/AD_{signature-}$ may be slightly inflated due to the limited representation of $A\beta+$ controls. Although all $A\beta+$ controls were below the $E\tau$ VOI cutoff in this data, it is routinely reported that cognitively normal $A\beta+$ subjects have elevated inferior temporal tau uptake [19, 35, 44]. One possibility for not observing this trend in this data might be the restrictive MMSE range (MMSE 29, 30) allowed in subjects classified as cognitively normal. We have imposed this strict MMSE threshold in order to obtain a clearer picture of tau levels in normal aging, considering the possibility that $A\beta+$ subjects with lower MMSE (e.g., 26 or 27) that might have been classified as cognitively unimpaired in other studies [19, 44] may actually be showing impairment consistent with the earliest stages of Alzheimer's disease. This data suggests that $E\tau+/AD_{signature-}$ subjects present an intermediate level of progression between $E\tau-/AD_{signature-}$ and $E\tau+/AD_{signature+}$ subjects. Accordingly, a natural extension of this work would be to explore if $E\tau+/AD_{signature-}$ subjects eventually convert to advanced disease subjects.

It is important to emphasize that the regions suggested in this work are not the only ones that might identify early AD subjects. Multiple studies have suggested individual temporal, composite, and temporoparietal regions to detect similar subgroups of subjects [19, 20, 26–29, 35, 45, 46]. Jack et al. have shown that their early AD meta-ROI consisting of fusiform and posterior cingulate best separates cognitively normal $A\beta-$ and $A\beta+$ subjects [27]. Likewise, Mishra et al. have found entorhinal cortex, lateral occipital cortex, inferior temporal, and amygdala as being important in differentiating between high and low tau preclinical AD subjects [47]. Johnson et al. report elevated tau uptake within the inferior temporal lobes of preclinical AD subjects, and Hanseeuw et al. report a greater increase in tau levels within the inferior temporal cortex of individuals with increasing $A\beta$ [25, 44]. We compared the $E\tau$ VOI with FreeSurfer-derived regions of the inferior temporal lobe, composite of the fusiform and posterior cingulate (similar to early AD meta ROI) [27], and composite of the amygdala, entorhinal cortex, fusiform, parahippocampal, inferior temporal, and middle temporal gyri (similar to temporal meta-ROI) [26]. We observed similar differences in baseline SUVR, 18-month change in SUVR, cortical thickness,

and MMSE. The performance of these regions varied slightly in detecting autopsy-confirmed Braak IV subjects. The inferior temporal lobe, $E\tau$ VOI, and AD meta-ROI-like and early AD meta-ROI-like VOIs identified 11/11, 10/11, 9/11, and 7/11 Braak IV subjects, respectively (Fig. S4A-D). Since the early AD meta-ROI does not sample from the inferior temporal region, we think its performance in identifying B2 NFT score subjects is slightly lower. Lowe et al. have shown that using the AD-centric meta-ROI [26], they were able to identify autopsy-confirmed Braak IV and higher subjects [48].

In this work, we have shown that the $E\tau$ VOI is not only sensitive in identifying Braak IV and higher subjects but also has good specificity (2/7 B1 NFT score subjects were identified). In addition, combining our $E\tau$ and AD_{signature} VOI, we can differentiate Braak IV subjects. In separate cohorts, we have also shown that these subjects (identified by the $E\tau$ VOI) progress within 18 months in terms of tau accumulation, neurodegeneration, and cognition. Within the data presented here, on average, tau was predominantly restricted to the set of regions selected.

Conclusion

The $E\tau$ VOI identified subjects with elevated temporal but not global tau that were primarily $A\beta+$, $APOE \epsilon 4$ carriers, and diagnosed as MCI or AD. $E\tau+/AD_{signature-}$ subjects had greater accumulation of tau, greater atrophy, and higher decline on MMSE, FAQ, and ADAS-Cog11 in 18 months compared to $E\tau-/AD_{signature-}$ subjects. Furthermore, the $E\tau+/AD_{signature-}$ subjects did not have elevated flortaucipir outside the medial/lateral temporal regions. Finally, the $E\tau$ VOI accurately identified the majority of the intermediate NFT score subjects in our autopsy-confirmed data. As far as we know, this is the first study that presents a visualization of ante-mortem FTP retention patterns that at a group level agree with the neurofibrillary tangle staging scheme proposed by Braak. Based on these findings, we conclude that the $E\tau$ VOI may be sensitive for detecting symptomatic subjects early in the course of Alzheimer's disease.

Supplementary Information

The online version contains supplementary material available at <https://doi.org/10.1186/s13195-023-01160-6>.

Additional file 1: Supplementary Figure S1.
Additional file 2: Supplementary Figure S2.
Additional file 3: Supplementary Figure S3.
Additional file 4: Supplementary Figure S4.
Additional file 5: Supplementary Table S1.

Acknowledgements

The authors would like to thank Deborah Dsouza, an employee of Syneos Health, and funded by Eli Lilly and Company for their editorial contributions.

Authors' contributions

V.K designed and performed the overall analyses and interpretations of the data, created the figures, and wrote the manuscript. S. S, M. N, I. K, M. L, A. M, J. Z, A. F, M. M, M. D, and M. P contributed to the data interpretation, designing of the analysis, intellectual contributions, and critical revision and writing of the manuscript. The authors read and approved the final manuscript.

Funding

This study was sponsored by Eli Lilly and Company. All authors are employees of Avid Radiopharmaceuticals and/or Eli Lilly and Company and may be minor stockholders in the company.

Availability of data and materials

Lilly provides access to all individual participant data collected during the trial, after anonymization, with the exception of pharmacokinetic or genetic data. Data are available to request 6 months after the indication studied has been approved in the USA and EU and after primary publication acceptance, whichever is later. No expiration date of data requests is currently set once data are made available. Access is provided after a proposal has been approved by an independent review committee identified for this purpose and after receipt of a signed data sharing agreement. Data and documents, including the study protocol, statistical analysis plan, clinical study report, and blank or annotated case report forms, will be provided in a secure data sharing environment. For details on submitting a request, see the instructions provided at www.vivli.org.

Declarations

Ethics approval and consent to participate

The study was reviewed and approved by appropriate local ethics committees, and written informed consent was obtained from study participants.

Consent for publication

N/A

Competing interests

All authors reported receiving stock options and a salary (as full-time employees) from Eli Lilly and Company.

Author details

¹Eli Lilly and Company, Indianapolis, IN 46285, USA.

Received: 26 October 2022 Accepted: 1 January 2023

Published online: 28 February 2023

References

- Hyman BT, Trojanowski JQ. Consensus recommendations for the postmortem diagnosis of Alzheimer's disease. The National Institute on Aging, and Reagan Institute working group on diagnostic criteria for the neuropathological assessment of Alzheimer's disease. *Neurobiol Aging*. 1997;18:S1–2.
- Nelson PT, Alafuzoff I, Bigio EH, Bouras C, Braak H, Cairns NJ, et al. Correlation of Alzheimer disease neuropathologic changes with cognitive status: a review of the literature. *J Neuropathol Exp Neurol*. 2012;71:362–81. <https://doi.org/10.1097/NEN.0b013e31825018f7>.
- Bouras C, Hof PR, Giannakopoulos P, Michel JP, Morrison JH. Regional distribution of neurofibrillary tangles and senile plaques in the cerebral cortex of elderly patients: a quantitative evaluation of a one-year autopsy population from a geriatric hospital. *Cereb Cortex N Y N*. 1991;1994(4):138–50. <https://doi.org/10.1093/cercor/4.2.138>.
- Montine TJ, Phelps CH, Beach TG, Bigio EH, Cairns NJ, Dickson DW, et al. National Institute on Aging-Alzheimer's Association guidelines for the neuropathologic assessment of Alzheimer's disease: a practical approach. *Acta Neuropathol (Berl)*. 2012;123:1–11. <https://doi.org/10.1007/s00401-011-0910-3>.

5. Hurtado DE, Molina-Porcel L, Iba M, Aboagye AK, Paul SM, Trojanowski JQ, et al. A β accelerates the spatiotemporal progression of tau pathology and augments tau amyloidosis in an Alzheimer mouse model. *Am J Pathol*. 2010;177:1977–88. <https://doi.org/10.2353/ajpath.2010.100346>.
6. Umeda T, Maekawa S, Kimura T, Takashima A, Tomiyama T, Mori H. Neurofibrillary tangle formation by introducing wild-type human tau into APP transgenic mice. *Acta Neuropathol (Berl)*. 2014;127:685–98. <https://doi.org/10.1007/s00401-014-1259-1>.
7. Clark CM, Pontecorvo MJ, Beach TG, Bedell BJ, Coleman RE, Doraiswamy PM, et al. Cerebral PET with florbetapir compared with neuropathology at autopsy for detection of neuritic amyloid- β plaques: a prospective cohort study. *Lancet Neurol*. 2012;11:669–78. [https://doi.org/10.1016/S1474-4422\(12\)70142-4](https://doi.org/10.1016/S1474-4422(12)70142-4).
8. Sabri O, Sabbagh MN, Seibyl J, Barthel H, Akatsu H, Ouchi Y, et al. Florbetaben PET imaging to detect amyloid beta plaques in Alzheimer's disease: phase 3 study. *Alzheimers Dement J Alzheimers Assoc*. 2015;11:964–74. <https://doi.org/10.1016/j.jalz.2015.02.004>.
9. Curtis C, Gamez JE, Singh U, Sadowsky CH, Villena T, Sabbagh MN, et al. Phase 3 trial of flutemetamol labeled with radioactive fluorine 18 imaging and neuritic plaque density. *JAMA Neurol*. 2015;72:287–94. <https://doi.org/10.1001/jamaneurol.2014.4144>.
10. Xia C-F, Arteaga J, Chen G, Gangadharath U, Gomez LF, Kasi D, et al. [¹⁸F]T807, a novel tau positron emission tomography imaging agent for Alzheimer's disease. *Alzheimers Dement J Alzheimers Assoc*. 2013;9:666–76. <https://doi.org/10.1016/j.jalz.2012.11.008>.
11. Hostetler ED, Walji AM, Zeng Z, Miller P, Bennacef I, Salinas C, et al. Preclinical characterization of 18F-MK-6240, a promising PET tracer for in vivo quantification of human neurofibrillary tangles. *J Nucl Med Off Publ Soc Nucl Med*. 2016;57:1599–606. <https://doi.org/10.2967/jnumed.115.171678>.
12. Mueller A, Bullich S, Barret O, Madonia J, Berndt M, Papin C, et al. Tau PET imaging with 18F-PI-2620 in patients with Alzheimer disease and healthy controls: a first-in-humans study. *J Nucl Med Off Publ Soc Nucl Med*. 2020;61:911–9. <https://doi.org/10.2967/jnumed.119.236224>.
13. Fleisher AS, Pontecorvo MJ, Devous MD, Lu M, Arora AK, Trucchio SP, et al. Positron emission tomography imaging with [¹⁸F]flortaucipir and postmortem assessment of Alzheimer disease neuropathologic changes. *JAMA Neurol*. 2020. <https://doi.org/10.1001/jamaneurol.2020.0528>.
14. Hyman BT, Phelps CH, Beach TG, Bigio EH, Cairns NJ, Carrillo MC, et al. National Institute on Aging-Alzheimer's Association guidelines for the neuropathologic assessment of Alzheimer's disease. *Alzheimers Dement J Alzheimers Assoc*. 2012;8:1–13. <https://doi.org/10.1016/j.jalz.2011.10.007>.
15. Pontecorvo MJ, Devous MD, Kennedy I, Navitsky M, Lu M, Galante N, et al. A multicentre longitudinal study of flortaucipir (18F) in normal ageing, mild cognitive impairment and Alzheimer's disease dementia. *Brain*. 2019;142:1723–35. <https://doi.org/10.1093/brain/awz090>.
16. Ossenkoppele R, Schonhaut DR, Schöll M, Lockhart SN, Ayakta N, Baker SL, et al. Tau PET patterns mirror clinical and neuroanatomical variability in Alzheimer's disease. *Brain*. 2016;139:1551–67. <https://doi.org/10.1093/brain/aww027>.
17. Schöll M, Lockhart SN, Schonhaut DR, O'Neil JP, Janabi M, Ossenkoppele R, et al. PET imaging of tau deposition in the aging human brain. *Neuron*. 2016;89:971–82. <https://doi.org/10.1016/j.neuron.2016.01.028>.
18. Buckley RF, Hanseeuw B, Schultz AP, Vannini P, Aghjayan SL, Properzi MJ, et al. Region-specific association of subjective cognitive decline with tauopathy independent of global β -amyloid burden. *JAMA Neurol*. 2017;74:1455–63. <https://doi.org/10.1001/jamaneurol.2017.2216>.
19. Johnson KA, Schultz A, Betensky RA, Becker JA, Sepulcre J, Rentz D, et al. Tau PET imaging in aging and early Alzheimer's disease. *Ann Neurol*. 2016;79:110–9. <https://doi.org/10.1002/ana.24546>.
20. Schultz SA, Gordon BA, Mishra S, Su Y, Perrin RJ, Cairns NJ, et al. Widespread distribution of tauopathy in preclinical Alzheimer's disease. *Neurobiol Aging*. 2018;72:177–85. <https://doi.org/10.1016/j.neurobiolaging.2018.08.022>.
21. Braak H, Alafuzoff I, Arzberger T, Kretschmar H, Del Tredici K. Staging of Alzheimer disease-associated neurofibrillary pathology using paraffin sections and immunocytochemistry. *Acta Neuropathol (Berl)*. 2006;112:389–404. <https://doi.org/10.1007/s00401-006-0127-z>.
22. Braak H, Braak E. Staging of Alzheimer's disease-related neurofibrillary changes. *Neurobiol Aging*. 1995;16:271–8 discussion 278–284.
23. Price JL, Morris JC. Tangles and plaques in nondemented aging and "preclinical" Alzheimer's disease. *Ann Neurol*. 1999;45:358–68.
24. Knopman DS, Parisi JE, Salviati A, Floriach-Robert M, Boeve BF, Ivnik RJ, et al. Neuropathology of cognitively normal elderly. *J Neuropathol Exp Neurol*. 2003;62:1087–95. <https://doi.org/10.1093/jnen/62.11.1087>.
25. Hanseeuw BJ, Betensky RA, Jacobs HLL, Schultz AP, Sepulcre J, Becker JA, et al. Association of amyloid and tau with cognition in preclinical Alzheimer disease. *JAMA Neurol*. 2019;76:915–24. <https://doi.org/10.1001/jamaneurol.2019.1424>.
26. Jack CR, Wiste HJ, Weigand SD, Therneau TM, Lowe VJ, Knopman DS, et al. Defining imaging biomarker cut points for brain aging and Alzheimer's disease. *Alzheimers Dement J Alzheimers Assoc*. 2017;13:205–16. <https://doi.org/10.1016/j.jalz.2016.08.005>.
27. Jack CR, Wiste HJ, Schwarz CG, Lowe VJ, Senjem ML, Vemuri P, et al. Longitudinal tau PET in ageing and Alzheimer's disease. *Brain*. 2018;141:1517–28. <https://doi.org/10.1093/brain/awy059>.
28. Ossenkoppele R, Rabinovici GD, Smith R, Cho H, Schöll M, Strandberg O, et al. Discriminative accuracy of [¹⁸F]flortaucipir positron emission tomography for Alzheimer disease vs other neurodegenerative disorders. *JAMA*. 2018;320:1151–62. <https://doi.org/10.1001/jama.2018.12917>.
29. Vogel JW, Mattsson N, Iturria-Medina Y, Strandberg OT, Schöll M, Dansereau C, et al. Data-driven approaches for tau-PET imaging biomarkers in Alzheimer's disease. *Hum Brain Mapp*. 2019;40:638–51. <https://doi.org/10.1002/hbm.24401>.
30. Jenkinson M, Bannister P, Brady M, Smith S. Improved optimization for the robust and accurate linear registration and motion correction of brain images. *Neuroimage*. 2002;17:825–41.
31. Joshi AD, Pontecorvo MJ, Lu M, Skovronsky DM, Mintun MA, Devous MD. A semiautomated method for quantification of F 18 flortaucipir PET images. *J Nucl Med*. 2015;56(11):1736–41. <https://doi.org/10.2967/jnumed.114.153494>. Epub 2015 Sep 3.
32. Pontecorvo MJ, Arora AK, Devine M, Lu M, Galante N, Siderowf A, et al. Quantitation of PET signal as an adjunct to visual interpretation of flortaucipir imaging. *Eur J Nucl Med Mol Imaging*. 2017;44:825–37. <https://doi.org/10.1007/s00259-016-3601-4>.
33. Southekal S, Devous MD, Kennedy I, Navitsky M, Lu M, Joshi AD, et al. Flortaucipir F 18 quantitation using parametric estimation of reference signal intensity. *J Nucl Med Off Publ Soc Nucl Med*. 2018;59:944–51. <https://doi.org/10.2967/jnumed.117.200006>.
34. Arora A, Pontecorvo MJ, Mintun MA, Fleisher A, Devous MD, Lu M, et al. Evaluation of a visual read method for flortaucipir PET scans. *Miami: Hum. Amyloid Imaging*; 2019. p. 129.
35. Sepulcre J, Schultz AP, Sabuncu M, Gomez-Isla T, Chhatwal J, Becker A, et al. In vivo tau, amyloid, and gray matter profiles in the aging brain. *J Neurosci Off J Soc Neurosci*. 2016;36:7364–74. <https://doi.org/10.1523/JNEUROSCI.0639-16.2016>.
36. Dale AM, Fischl B, Sereno MI. Cortical surface-based analysis. I. Segmentation and surface reconstruction. *Capital Neuroimage*. 1999;9:179–94. <https://doi.org/10.1006/nimg.1998.0395>.
37. Desikan RS, Ségonne F, Fischl B, Quinn BT, Dickerson BC, Blacker D, et al. An automated labeling system for subdividing the human cerebral cortex on MRI scans into gyral based regions of interest. *Neuroimage*. 2006;31:968–80. <https://doi.org/10.1016/j.neuroimage.2006.01.021>.
38. Abdi H, Williams LJ, Beaton D, Posamentier MT, Harris TS, Krishnan A, et al. Analysis of regional cerebral blood flow data to discriminate among Alzheimer's disease, frontotemporal dementia, and elderly controls: a multi-block barycentric discriminant analysis (MUBADA) methodology. *J Alzheimers Dis JAD*. 2012;31(Suppl 3):S189–201. <https://doi.org/10.3233/JAD-2012-112111>.
39. Devous MD, Joshi AD, Navitsky M, Southekal S, Pontecorvo MJ, Shen H, et al. Test-retest reproducibility for the tau PET imaging agent flortaucipir F 18. *J Nucl Med*. 2018;59:937–43. <https://doi.org/10.2967/jnumed.117.200691>.
40. Jack CR, Petersen RC, Xu YC, Waring SC, O'Brien PC, Tangalos EG, et al. Medial temporal atrophy on MRI in normal aging and very mild Alzheimer's disease. *Neurology*. 1997;49:786–94. <https://doi.org/10.1212/WNL.49.3.786>.
41. Jack CR, Petersen RC, Xu Y, O'Brien PC, Smith GE, Ivnik RJ, et al. Rate of medial temporal lobe atrophy in typical aging and Alzheimer's disease. *Neurology*. 1998;51:993–9. <https://doi.org/10.1212/WNL.51.4.993>.
42. Marqué M, Siao Tick Chong M, Antón-Fernández A, Verwer EE, Sáez-Calveras N, Meltzer AC, et al. [F-18]-AV-1451 binding correlates with

- postmortem neurofibrillary tangle Braak staging. *Acta Neuropathol (Berl)*. 2017;134:619–28. <https://doi.org/10.1007/s00401-017-1740-8>.
43. Smith R, Wibom M, Pawlik D, Englund E, Hansson O. Correlation of in vivo [18F] flortaucipir with postmortem Alzheimer disease tau pathology. *JAMA Neurol*. 2019;76:310–7. <https://doi.org/10.1001/jamaneurol.2018.3692>.
 44. Johnson K, Schultz AP, Raman R, Sperling RA. Tau PET in A4: preliminary report. *Tau PET A4 Prelim. Rep*: Chicago; 2018.
 45. Schwarz AJ, Shcherbinin S, Slieker LJ, Risacher SL, Charil A, Irizarry MC, et al. Topographic staging of tau positron emission tomography images. *Alzheimers Dement Diagn Assess Dis Monit*. 2018;10:221–31. <https://doi.org/10.1016/j.dadm.2018.01.006>.
 46. Maass A, Landau S, Baker SL, Horng A, Lockhart SN, La Joie R, et al. Comparison of multiple tau-PET measures as biomarkers in aging and Alzheimer's disease. *NeuroImage*. 2017;157:448–63. <https://doi.org/10.1016/j.neuroimage.2017.05.058>.
 47. Mishra S, Gordon BA, Su Y, Christensen J, Friedrichsen K, Jackson K, et al. AV-1451 PET imaging of tau pathology in preclinical Alzheimer disease: defining a summary measure. *NeuroImage*. 2017;161:171–8. <https://doi.org/10.1016/j.neuroimage.2017.07.050>.
 48. Lowe VJ, Lundt ES, Albertson SM, Min H-K, Fang P, Przybelski SA, et al. Tau-positron emission tomography correlates with neuropathology findings. *Alzheimers Dement*. 2020;16:561–71. <https://doi.org/10.1016/j.jalz.2019.09.079>.

Publisher's Note

Springer Nature remains neutral with regard to jurisdictional claims in published maps and institutional affiliations.

Ready to submit your research? Choose BMC and benefit from:

- fast, convenient online submission
- thorough peer review by experienced researchers in your field
- rapid publication on acceptance
- support for research data, including large and complex data types
- gold Open Access which fosters wider collaboration and increased citations
- maximum visibility for your research: over 100M website views per year

At BMC, research is always in progress.

Learn more biomedcentral.com/submissions

